Calcineurin-mediated regulation of GAP-43 is essential for neurite and synapse formation and protects against α-synuclein-induced degeneration

Sofia Zaichick[1#], Ekaterina Grebenik[1#] and Gabriela Caraveo[1*].

[1] Department of Neurology, Feinberg School of Medicine, Northwestern University, Chicago, IL 60611

# equal contribution

* Corresponding author, gabriela.piso@northwestern.edu

ABSTRACT

Rise in calcium (Ca^{2+}) and hyperactivation of Ca^{2+}-dependent phosphatase calcineurin are two key determinants of α-synuclein (α-syn) pathobiology implicated in synucleinopathies such as Dementia with Lewy Bodies and Parkinson's Disease. Calcineurin activity can be inhibited with FK506, a Food and Drug Administration (FDA)-approved compound. Our previous work demonstrated a protective effect of sub-saturating doses of FK506 against α-syn pathology in a rat model of α-syn neurodegeneration. This neuroprotection was associated with the phosphorylation of GAP-43. In this study, we present evidence that phosphorylation of GAP-43 regulated by calcineurin is a critical determinant for neurite branching and synapse formation. Phosphorylation of GAP-43 promotes neurite branching and synapse formation whereas dephosphorylation prevents it. Therefore, our findings provide a novel way in which GAP-43 activity can be regulated by calcineurin and provide the mechanistic basis for neuroprotection for FK506 effects in neurons experiencing α-syn proteotoxic stress.

Key words: α-synuclein, calcineurin, FK506, neuroprotection, GAP-43, neurite branching, synapses

INTRODUCTION

Misfolding of the small lipid binding protein α-synuclein (α-syn), plays a central role in a group of neurological diseases collectively known as synucleinopathies [1]. These encompass Parkinson's Disease (PD), Multiple Systems Atrophy and two prominent Lewy Body Dementias: Dementia with Lewy Bodies (DLB) and Parkinson's Disease Dementia (PDD). Using a diverse array of

model systems, we and others have found that α-syn leads to a pathological increase in cytosolic Ca^{2+} and a subsequent hyperactivation of calcineurin (CaN), the highly evolutionary conserved Ca^{2+}-Calmodulin-dependent serine/threonine phosphatase resulting in cell death [2-14]. Importantly, we found that reducing CaN activity by genetic means or with sub-saturating doses of the CaN-specific inhibitor, FK506 (also known as Tacrolimus), rescues cells against the toxic effects of α-syn [12,6].

FK506 is a well-established drug and is already in widespread clinical use at high doses to suppress the rejection of organs in transplant patients, a process in which CaN also plays a critical role [15]. Importantly, we found that sub-saturating doses of FK506 have excellent, long lasting brain penetrance and rapid clearance from the blood preventing potential adverse side effects [6]. With a weekly dosing regimen, we embarked into a large *in vivo* study using a rat model of PD based on a unilateral injection of α-syn into Substantia Nigra Pars Compacta (SNc) [6]. For analysis, animals were stratified based on their final content of FK506 in the brain. We found that only sub-saturating doses of FK506 (<5ng/ml) were enough to prevent neurodegeneration by ameliorating the deficits in motor behavior, dopamine and dopamine transporter levels in the striatum caused by α-syn [6]. To identify the substrates dephosphorylated by calcineurin associated with the toxic vs protective responses we took an unbiased phospho-proteomic approach using Tandem Mass Tags (TMT) MS from striatal tissue of these animals[6].

Here we show that GAP-43 phosphorylation, a protein known to be important in growth cone pathfinding during neuronal development and in the adults upon injury [16,17], is regulated by α-syn and CaN. Using phosphomutants of the α-syn- and CaN-sensitive phosphorylation sites in cell lines and primary cortical neurons, we show that GAP-43 phosphorylation is critical for neurite branching and synapse formation. GAP-43 phosphomimetic mutant, which mimics the CaN inhibition, enables neurite branching and synapse formation; the GAP-43 phosphoablative mutant on the other hand, which mimics the α-syn condition with constitutive CaN activity, does not. Moreover, we found that the α-syn- and CaN- sensitive phosphorylation sites serve as a scaffold for proteins enriched in ribosomal function. Importantly, overexpression of the GAP-43 phosphomimetic mutant rescued the neuronal toxicity caused by α-syn by increasing ATP levels, number of neurons and PSD95 levels. Thus, our findings reveal a novel mechanism by which CaN regulates GAP-43 activity and provide a basis for the neuroprotective effects of FK506 in neurons.

RESULTS

Using TMT MS from the striatal tissue of α-syn animals treated with sub-saturating doses of FK506, we detected 51 of 3,526 phosphopeptides that changed significantly when comparing α-syn animals to control [6]. Of these, half were significantly hypo-phosphorylated in α-syn animals. Because CaN is a phosphatase that is highly activated under increased levels of α-syn, we focused on the hypo-phosphorylated peptides for the analysis. Of these, only four phosphopeptides decreased their phosphorylation to control levels in the presence of sub-saturating doses of FK506. These belonged to GAP-43 (known as F1, neuromodulin, B-50, G50 and pp46) and BASP1 (also known as NAP-22, CAP-23) [6] (Fig.1A).

GAP-43 and BASP1 are functionally related proteins essential for neuronal development due to their roles in growth cone pathfinding [16]. Moreover, these proteins play critical roles in neuronal regeneration and plasticity following injury [17]. Their ability to promote growth cone formation is attributed to their regulation of actin dynamics and vesicle recycling at presynaptic terminals [18,19]. One way in which GAP-43 activity, and consequently its effect on neurite outgrowth can be regulated, is through phosphorylation by Protein Kinase C (PKC) and dephosphorylation by CaN at serine 41 (S41) [20, 21, 22,23].

To determine the relevance of the phosphorylation sites identified through our unbiased TMT-MS approach (S86, T95, and T172 of GAP-43) for neurite growth, we generated phosphomimetic and phosphoablative mutants of all the CaN-sensitive sites in GAP-43. We began by testing the mutants in PC12 cells, a rat pheochromocytoma cell line capable of differentiating into neuronal-like cells upon the addition of soluble Nerve Growth Factor or transfection with nerve growth proteins such as GAP-43[24]. PC12 cells were co-transfected with GFP (green fluorescent protein) to better visualize neurites) and GAP-43 in either wild type (WT), or phosphomutant form of the previously identified site S41 as a positive control, or our newly identified CaN-sensitive sites S86, T95, and T172. Cells were imaged 24 hours post-transfection and analyzed for the length of the longest neurite and the number of branches per neurite. As expected, overexpression of WT and the phosphomimetic-S41 mutant of GAP-43 increased neurite length compared to GFP alone (Fig. 1B), whereas the CaN-dependent phosphoablative-S41 mutant diminished this effect (Fig. 1B). Similarly, the phosphomimetic-S86 and phosphomimetic-T172 mutants of GAP-43 also increased neurite length comparable to WT GAP-43, while the phosphoablative-S86 and phosphoablative-T172 mutants diminished this effect (Fig. 1B). Regarding neurite branching, only the phosphomimetic-S86 and phosphomimetic-T172 mutants increased branching compared to

WT GAP-43, with a synergistic effect observed for the double phosphomimetic-S86,T172 mutant, comparable to the phosphomimetic-S41 mutant. In contrast, the CaN-dependent phosphoablative single and double mutants (S86 and T172) showed no effect (Fig. 1C). Notably, these morphological changes were not due to changes in protein expresion (Fig.2A). These data show that the S86,T172 CaN-sensitive phosphosites on GAP-43, identified in an unbiased phosphoproteomic screen in a model of α-syn pathology, can modulate neurite branching.

We next asked if the effect on neurite branching, we observed in PC12 cells, can be recapitulated in primary cortical neurons. Rat cortical neurons were infected with lentiviruses expressing fusion proteins of GFP with either WT GAP-43, or the double phosphomimetic and phosphoablative mutants of S86,T172 phosphosites (hereafter referred to as phosphomimetic and phosphoablative double mutants). The actin cytoskeleton was visualized using BODIPY 558/568 Phalloidin, which binds to F-actin, allowing fluorescence microscopy-based observation of actin fibers. Sholl analysis was performed to monitor neurite branching. Expression of WT GAP-43 caused a marginal increase in actin cytoskeleton complexity and neurite branching compared to GFP alone (Fig. 2B,C). In contrast, the phosphomimetic double mutant further enhanced actin cytoskeleton complexity, resulting in a significantly increased dendritic arborization compared to WT GAP-43 (Fig.2B,C). Importantly, this effect was phosphorylation-dependent, as the phosphoablative double mutant did not show an increase in branching complexity (Fig. 2B,C).

Given that the actin cytoskeleton was affected by GAP-43 CaN-dependent mutants, we investigated the effect of GAP-43 in dendritic spines, as they are highly dependent on actin dynamics. Expression of WT and phosphomimetic double mutant GAP-43 increased the total number of spines relative to phosphoablative double mutant and to GFP alone (Fig. 2D). While the changes in spine number where dependent on S86,T172 phosphoryaltion, the morphological patterns (mushroom, stubby, filipodia and thin-like dendritic spines) were not significantly different between GFP, and WT and CaN-dependent phosphomutants GAP-43 (Fig. 2E). However, the pattern of GAP-43 localization within spines appears to be very different between the CaN-dependent phosphomutants (Fig.2 F). The phosphoablative double mutant is less expressed and diffused through the spine compared to phosphomimetic double mutant and the WT which are highly expressed in the spines (Fig.2F). Together, these data indicate that the CaN-sensitive sites S86,T172 are critical to promote branching and spine formation in primary cortical neurons.

To identify protein interactors responsible for the neurite branching and spine effects of GAP-43 we took an immunoprecipitation (IP) MS-based approach, utilizing four different experimental conditions: WT, phosphoablative double mutant, phosphomimetic double mutant GAP-43-GFP and GFP alone to control for nonspecific protein copurification. HeLa cells were transfected with these constructs and IP using anti-GFP antibodies. GAP-43 IP were robust and, importantly, recovered similar amounts of GAP-43 across WT and the phosphomutants (supplemental Table 1). Positive hits were considered those that either were present in the GAP-43 pulldowns and not in the GFP alone pulldowns or, if present in the GFP alone pulldown, those hits that were statistically significant to GAP-43-specific pulldowns. Under these criteria, we retrieved a total of 31 candidates for GAP-43-interacting partners that scored as positive hits. GAP-43 WT shared 6 protein interactors with the phosphoablative mutant, which were enriched for proteins involved in rRNA processing and structural components of ribosomes. In contrast, only one interactor, NPM1—a protein involved in ribosome nuclear export—was shared between the WT and the phosphomimetic mutant (Fig. 3A,B). Additionally, 24 protein interactions were enriched in the phosphoablative mutant, which were also enriched for proteins involved in rRNA processing, structural ribosomal components, and cadherin binding (Fig. 3A,B). Together, these findings suggest that the CaN-dependent phosphorylation sites mediate interactions with ribosomal proteins to regulate neurite outgrowth.

Phosphorylation at S86 and T172 was associated with neuroprotection in α-syn rats treated with FK506 [6] (Fig.1A). To investigate if the effects of GAP-43 phosphomimetic double mutant in the dendritic arbor could protect against α-syn toxicity, we co-transduced primary cortical neurons with the disease-associated form of α-syn, A53T [25], or with an empty vector as control, along with GAP-43 WT and CaN-dependent double phosphomutants (Fig. 4A). Five weeks post infection, we immunostained the cultures for the neuronal specific marker MAP2 to determine the number of neurons after each condition. In addition, we measured ATP levels as an alternative surrogate for viability. While overexpression of GAP-43 WT or GAP-43 phosphoablative double mutant did not have an effect in α-syn, as measured by MAP2 and ATP, overexpression of the phosphomimetic double mutant protected the neurons against the toxic effects of α-syn (Fig. 4B-D). Moreover, the protective effects of the phosphomimetic double mutant were associated with an increase in PSD-95 (postsynaptic density protein 95, Fig. 4E,F). PSD-95 is highly abundant at postsynaptic spines, where it anchors and organizes N-methyl-D-aspartate receptors and other synaptic proteins critical for synaptic plasticity. Together, these findings suggest that

phosphorylation at the CaN-dependent phosphorylation sites S86 and T172 can regulate α-syn pathobiology.

DISCUSSION

Using an unbiased phosphoproteomic approach, we identified GAP-43 as one of the two prominent substrates regulated by CaN in the striatum of a rat model of α-syn pathology. Dephosphorylation at S86,T172 of GAP-43 was associated with α-syn pathology, whereas phosphorylation at these sites was associated with the neuroprotection due to partial inhibition of CaN [26]. Although these same sites were identified in previous phosphoproteomic screens[27] associated with physiological neurite outgrowth[28,29], their causal role in regulating GAP-43 activities, nor their role in disease had been investigated. Using a genetic approach through phosphomutants we specifically dissected the contribution of these phosphorylation to neurite growth. We showed that phosphorylation of GAP-43 at S86 and T172 (mimicked by the phosphomimetic mutants), increased neurite branching and spine density, whereas constitutive dephosphorylation of GAP-43 by CaN (mimicked by the phosphoablative mutants) decreased it. Furthermore, we discovered that phosphorylation at these CaN-sensitive sites facilitates the recruitment of ribosomal proteins. Interestingly, several other studies, have established that the ribosomal apparatus is necessary to carry out protein synthesis that supports dendritic growth and maintenance [30,31,32,33,34,35]. Our studies suggest that phosphorylation at S86 and T172 enable dendritic and spine growth by recruiting the translation machinery to support protein synthesis at growth cones.

Regulation of GAP-43 has been explored as a therapeutic strategy for neurodegenerative diseases. Specifically, the effects of agents that upregulate GAP-43, such as BDNF, have been tested in animal models of PD[36]. BDNF treatment has been shown to ameliorate behavioral impairments[37]. Treatments with Pilose antler extracts in a rat model of PD, increased striatal GAP-43 protein expression and reduced dopaminergic SNc neuronal cell death[38]. In a scratch lesion model *in vitro* using A53T α-syn, reduced neurite regeneration and subsequent dopaminergic neuronal loss were associated with decreased striatal GAP-43 expression [39]. Consistent with these findings, reduced GAP-43 expression has been observed in cerebrospinal fluid [40] and in SNc postmortem sections from PD patients[41]. Despite the positive effects of neurotrophic factors in animal models, their short half-life, low bioavailability, and limited permeability through the blood-brain barrier (BBB) imposed challenges in their application to patients [37]. Such challenges associated with using neurotrophic factors to increase GAP-43 levels can be avoided by using

other pharmacological agents that can cross the BBB and modulate their activities, for instance, via phosphorylation. A potential candidate is the FDA-approved CaN inhibitor FK506.

We demonstrated that the increase in dendritic branching and spine density induced by the GAP-43 S86,T172 phosphomimetic mutants provides protection against α-syn toxicity. The phosphomimetic form of GAP-43 at S86,T172 sites mimics the conditions observed in the rat α-syn animal model we treated with FK506 and provides a mechanistic explanation for the neuroprotective benefits of CaN inhibition observed *in vivo*[6]. In the rat model of PD we used, we showed that FK506 can cross the BBB, alter phosphorylation of GAP-43, and confer neuroprotection at doses 10-fold lower than the standard immunosuppressive dose [6]. At sub-immunosuppressive doses, the risk of secondary effects, such as opportunistic infections, posterior reversible leukoencephalopathy, and seizures typically achieved at clinical doses would be avoided. Moreover, these sub-saturating FK506 doses would finely tune GAP-43 to drive sufficient, but not hyperactive, dendritic sprouting in a spatially and temporally confined manner. This regulation is necessary to promote regeneration specifically in the affected neuronal populations at the right time window while preventing potential complications arising from hyperconnectivity. Further exploration of these areas will facilitate the development of GAP-43-targeting therapies for neurodegenerative diseases.

MATERIALS AND METHODS

Plasmids and viruses

Lentiviral Plasmids: pLV-αSyn A53T (hSynapsin promoter) was a generous gift from Aftabul Haque and Susan Lindquist (Whitehead Institute for Biomedical Research, Cambridge, MA). Control (empty vector) plasmid was generated by excising αSyn and ligating the resulted product. Murine GAP-43-FLAG pAG plasmid was a generous gift from Eric Norstrom (DePaul University Chicago). The GAP-43 mutagenesis was performed using Q5 Site-Directed Mutagenesis Kit (E0554, New England Biolabs) according to the manufacturer protocol. Murine GAP-43-FLAG pcDNA 3.1/Hygro construct was used as a template DNA. T95, S86 and T172 were substituted with either A or EE; S41 was substituted with either A or DD.

For the experiments with primary cortical neurons, GAP-43 WT and single phosphoablative and phosphomimetic mutants S41A and S41DD (referred to as S41D in the main text), as well as double phosphomutants S86EE,T172EE (referred to as S86E,T172E in the main text) and S86A,T172A were subcloned into the lentiviral expression vector pLV-eGFP. Viruses were

produced in the laboratory and in the NU Gene editing transduction and Nanotechnology Core. In the laboratory, packaging plasmids (pMD2.G and psPAX2) were obtained from Addgene. Lentiviral constructs were packaged via lipid-mediated transient transfection of the expression constructs and packaging plasmids (pMD2.G and psPAX2) into HEK293T cells using a modified protocol from Park et al. [44]. Lentiviruses were purified and concentrated using the LentiX Concentrator (Clontech, PT4421-2) according to the manufacturer's protocol. Lentivirus titer was determined using the QuickTiter Lentivirus titer kit (lentivirus-associated HIV p24; Cell Biolabs, VPK-107) or HIV-1 p24 ELISA pair set (Sino Biological Inc, SEK11695) according to the manufacturer's protocol. All titers were further normalized in SH-SY5Y cells infected with gradual multiplicities of infection (MOI) volumes of lentivirus and processed for Western blot analysis 3 dpt. Equal MOIs were used to infect rat cortical cultures on 5DIV.

Cell lines

PC12 cells were maintained up to passage 10 in DMEM high glucose media supplemented with 10% NuSerum and 1% FBS. 70-80% confluent culture was passaged by trypsinization (0.05% Trypsin/EDTA) followed by centrifugation at 500 g for 5 min and resuspension in full culture medium. For the evaluation of the response to GAP-43 overexpression, the cells were seeded on collagen-coated tissue culture polystyrene. 1 ml aqueous solution containing 35 ug/ml human placenta collagen IV (Advanced Biomatrix) and 15 ug/ml chicken collagen II (Sigma) was added to each well of a 24-well plate followed by overnight air-drying at 25 °C and UV-sterilization. Lipofectamine 3000-assisted transfection was performed 24 h prior to examination. 500 ng pcDNA 3.1/Hygro construct (EV, GAP-43-FLAG WT, phosphoablative S86A,T172A mutant, or phosphomimetic S86EE,T172EE mutant) and 83 ng pEGFP-C1 were added to 50 µl Opti-MEM along with 0.8 ml P3000™ reagent. 0.8 µl of Lipofectamine 3000 reagent was diluted in 50 µl Opti-MEM in a separate sterile Eppendorf tube. Ater 5 min incubation, the DNA and Lipofectamine 3000 reagent solutions were combined, incubated for 30 min and then added to the wells of a 24-well plate with the PC-12 cells precultured for 24 h. After 5 h, the solution was replaced with the full growth media.

HeLa and HEK293T (human embryonic kidney cells) cells were cultured at 37°C and 5% CO_2 in Dulbecco's Modified Eagle Medium (DMEM) with 4.5% glucose (Corning), 10% Fetal Bovine Serum (Denville) and 1X penicillin and streptomycin (Gibco).

Primary Cortical Cultures

Embryonic rat cortical neurons were isolated from euthanized pregnant Sprague–Dawley rats at embryonic day 18 using a modified protocol from Lesuisse and Martin [42,43]. Protocol was approved by Northwestern University administrative panel on laboratory animal care. Embryos were harvested by Cesarean section and cerebral cortices were isolated and dissociated with 0.25% Trypsin without EDTA (Invitrogen, 15090-046) digestion for 15 min at 37°C and trituration with 1 ml plastic tip. Poly-D-Lysine (Sigma, P-1149)-coated 96-well and 24-well plates were seeded with 4×10^4 and 2×10^5 cells accordingly in neurobasal medium (Invitrogen, 21103-049) supplemented with 10% heat-inactivated FBS (Gibco), 0.5 mM glutamine (Gibco), penicillin (100 IU/mL), and streptomycin (100 µg/mL) (Gibco). Before seeding, cells were counted using the Automated cell counter TC10 (Bio-Rad) and viability (90-95%) was checked with Trypan Blue Stain (0.4%, Gibco 15250-061). After 1 hour (h) incubation at 37°C, media was changed to neurobasal medium (Invitrogen, 21103-049) supplemented with B27 (Invitrogen 17504044), 0.5 mM glutamine, penicillin (100 IU/mL), and streptomycin (100 µg/mL). One-half (out of 100 µl volume for 96-well plates and 500 µl volume for 24-well plates) of the media was changed 4 h before transduction on day 5 *in vitro* (5DIV). As a surrogate marker of cell viability, cellular ATP content was measured two-three times a week between 5-7.5 weeks post transduction using the ViaLight Plus kit (Lonza, LT07-221) or ATPlite kit (PerkinElmer, 6016941) according to the manufacturer's instructions.

Western blot

Infected neuronal cultures (5w2d post transduction) were lysed using a radioimmunoprecipitation (RIPA) assay buffer (50mM Tris/HCl pH 7.6; 150mM NaCl; 20mM KCl; 1.5mM MgCl2; 1% NP40; 0.1% SDS). In all experiments, lysis buffer was supplemented with the Halt protease and phosphatase inhibitor cocktail (Thermofisher; 78441). Samples were incubated on ice for 30 minutes and pushed through a 27G needle (10 times) to ensure full lysis. Samples were then centrifuged at 21,000 x g for 20 minutes and the obtained supernatants were used for Western blot analysis. Protein concentration was analyzed with the Pierce BCA Protein Assay kit (Thermofisher) and Fisherbrand™ accuSkan™ GO UV/Vis Microplate Spectrophotometer (Fisher Scientific). After the addition of the appropriate amount of the 6x Laemmli Sample Buffer (Bioland scientific LLC, sab03-02) with 5% ß-mercaptoethanol (Sigma) protein samples (10-30 µg) were boiled and separated on precasted 4-20% Criterion TGX Stain-free gels (Bio-Rad) and transferred to a nitrocellulose membrane (Amersham Protran 0.2um NC, #10600001). Membranes were blocked with 5% non-fat milk in 1X Tris-buffered saline (TBS) (50 mM Tris, pH 7.4, 150 mM NaCl) for 1 h at 25°C. Membranes were subsequently immunoblotted overnight in primary antibodies

(anti-α-Synclein, BD, 610787; anti-Actin, Abcam, ab6276, anti-PSD95, Thermofisher, MA1-046) at 4°C, shaking. The following day, the membranes were washed three times with 1X TBST (TBS with 0.1% Tween) for 5 minutes each and incubated in secondary IRDye antibodies for 1 h shaking at 25°C. Membranes were washed three times with 1X TBST for before imaging using Li-Cor Odyssey® CLx Imaging System. Images were processed using Image Studio Software (LI-COR Biosciences) and signal densities were quantified using Fiji [45].

Immunofluorescence

Transduced neuronal cultures (4-5 weeks post transduction, 96-well plates) were fixed with 3% (vol/vol) paraformaldehyde. Cells were then washed three times with 1X PBS for 5 minutes each wash and permeabilized using in 0.1% Triton X-100 in 1X PBS (PBST), at 25°C for 20min and then blocked in 2% Bovine Serum Albumin (BSA, Sigma, SLBT8252) in 1X PBST for at least 60 min at RT. Primary antibody (anti-MAP2, Millipore, AB5622) were diluted in the blocking buffer and incubated overnight at 4°C followed by triple wash and incubation (1-2 h at RT) with secondary antibodies, also diluted in the blocking buffer. Subsequently, cells were washed trice and incubated with Hoechst (Invitrogen, 33342) for 10 min at 25°C followed by triple rinsing with 1X PBS. Cells were imaged using Leica DMI3000B microscope fitted with an QImaging QIClick CCD Camera and Leica HCX PL FLUOTAR L 20X/0.40 CORR PH1 objective. Image acquisition was done using Q-capture pro7 software and manual tracking of the equal exposure and digital gain setting between images. All image processing and analysis was done using Fiji [45]. All experiments were done three independent times. Images were recorded from at least 4 wells and analyzed in a randomized and blinded fashion. MAP2-positive cell bodies (neurons) were manually calculated and subtracted from the total nuclei count (Hoechst). Fluorescence quantification was done using a Microplate Reader Infinite® M1000 PRO (Tecan) using appropriate excitation and emission wavelengths. Images were processed using ImageJ/FIJI software built-in package for color deconvolution (ABC-DAB) and processed for average intensity. Intensity values over six fields for each sample are compared and processed for statistical analysis.

Scholl analysis and spine determination

Scholl analysis was performed in 21DIV primary rat cortical neurons. The neurons were fixed with 4% formaldehyde in PBS for 15 minutes at 25 °C. Subsequently, the cells were washed with PBS trice for 5 min each and permeabilized with 0.1% Triton X-100 in PBS for another 15 minutes. The cells were washed twice with PBS and then stained with 165 nM BODIPY 558/568 Phalloidin

prepared in PBS with 1% BSA for one hour at 25 °C in the dark. After the staining, the cells were washed with PBS trice for 5 min each and mounted on coverslips. The neurons were imaged using Nikon A1R GaAsP point-scanning laser confocal microscope using 63x oil-immersion objective (NA = 1.4) with z-series of 8–10 images, taken at 0.3 µm intervals, with 1024 × 1024 pixel resolution. The stacks were then flattened to 1 image in ImageJ and Scholl Analysis performed using the SNT plugin (ImageJ) after manual tracing.

Dendritic spines were imaged using Nikon A1R GaAsP point-scanning laser confocal microscope using a 63× objective (NA = 1.4). Morphometric analysis was performed on spines from two dendrites (secondary or tertiary branches), totaling 100 µm, from each neuron. Single dendritic spines were determined from the intensity of BODIPY 558/568 Phalloidin. Mushroom-shaped spines were considered as head/neck ratio >1.1 and spine diameter >1 micron (spine area>0.78µm^2). For each condition, 10–16 neurons from at least 3 separate experiments were used.

Immunoprecipitation (IP) with GFP Trap beads

HeLa cells were transiently transfected with pER4-GFP and GAP-43 (WT and double phosphomutants S86A,T172A and S86D,T172E) subcloned in pER4-GFP vector. Lipid-mediated transient transfection was performed using Lipofectamine 2000 (Thermofisher, L3000015) according to the manufacturer's protocol. 24 hours post-transfection, the cells were briefly washed with ice-cold 1X PBS and lysed using 1% Triton X-100, 10% glycerol, 10 mM Tris/Cl pH 7.5; 150 mM NaCl, 0.5 mM EDTA. Lysis buffer was supplemented with the Halt protease and phosphatase inhibitor cocktail (Thermofisher; 78441). Samples were incubated on ice for 30 minutes and pushed through a 27G needle (10 times) to ensure full lysis and then centrifuged at 21,000 x g for 20 minutes. Protein concentration was analyzed with the Pierce BCA Protein Assay kit (Thermofisher). Each supernatant was incubated rotating at 4°C for 2 h with 30 ul of 50% slurry GFP-Trap beads (ChromoTek GFP-Trap® Agarose beads) prepared in lysis buffer. Next, the beads were washed trice in a centrifuge (2,500xg, 2 min, 4°C) with lysis buffer and two more times – with the wash buffer (10mM Tris-Cl pH7.5, 150mM NaCl, 0.5mM EDTA). IP samples were submitted for TMT-MS at the MIT Kock Proteomics facility.

Statistical Analysis

One-way ANOVA with Tukey's post hoc test was used for three or more dataset quantifications. Statistical calculations were performed with GraphPad Prism 7 Software (http://www.graphpad.com), p values <0.05 were considered significant. To correct for multiple

comparisons, in MS data analysis, the two-stage linear step-up procedure of Benjamini, Krieger and Yekutieli post-hoc tests was used to control the false discovery rate (FDR) and assess differences between phosphomutants, q = 0.05. Results are expressed as average + the standard error mean (SEM). Regression analysis was done using Microsoft Excel Statistics add-in package. A minimum of two independent biological replicates were used for each experiment with at least six replicates per sample within each experiment. The specific number of biological replicates for each experiment is listed in the figure legends.

FIGURE LEGENTS

Figure 1. **Calcineurin-dependent phosphosites S86 and T172 of GAP-43 contribute to neurite branching in PC12 cells**. **(A)** Phosphopeptides were analyzed from striatal samples of control, α-syn, and α-syn rats treated with <5 ng/mL of FK506. Samples were analyzed using TMT-MS, and peptides significantly rescued by FK506 treatment are presented. The identified phosphorylation site is highlighted in red. Data represent n= 3 rats. *p< 0.05 (two-tailed t-test). **(B-C)** PC12 cells were co-transfected with GFP and empty vector or GAP-43 in Wild type (WT) or the indicated phosphomutant form. The analysis includes measurements of the longest neurite **(B)** and the number of branches **(C)** from >300 cells across 4 independent experiments. All experiments are normalized relative to GFP control (in red; each line represents +/- SEM); WT GAP-43 serves as reference (in black; each line represents +/- SEM). *p< 0.05 comparison between phosphomimetic and phosphoablative mutants and •p< 0.05 comparison between phosphomutants and WT; One-way Anova with post hoc Tukey's test.

Figure 2. Calcineurin-dependent phosphosites S86 and T172 of GAP-43 contribute to neurite branching and spine formation in primary cortical neurons. **(A)** Representative western blot showing GFP expression in primary rat cortical neurons transfected with GFP alone, GFP fused to GAP-43 Wild-type (WT), or the indicated phosphomutants. Actin is used as a loading control. **(B)** Representative confocal images of rat primary cortical neurons transduced with GFP or GFP fusions of GAP-43 WT, phosphoablative mutants (S86A, T172A), or phosphomimetic mutants (S86D,T172E) at the CaN-dependent phosphorylation sites. Cultures were immunostained for GFP (green channel) and actin using BODIPY 558/568 Phalloidin (red). **(C)** Sholl analysis based on actin from cultures in (B). N= 6. **(D)** Total number of spines/10μm from conditions in (B). **(F)** Distribution of spine morphology from cultures in (B). **(E)** Representative images of dendritic spines from cultures in (B) 63X; scale bar is 10μm. In all conditions, SEM and *p< 0.05 One-way Anova with post hoc Tukey's test.

Figure 3. Calcineurin-dependent phosphosites S86 and T172 of GAP-43 bind structural components of ribosomes. **(A)** Venn diagram representation of all MS hits that passed the selection criteria described in main text and materials and methods. n = 3. One-Way Anova with a multi-comparison test using a two-stage linear step-up procedure of Benjamini, Krieger, and Yekutieli, q = 0.05. **(B)** Gene ontology analysis for molecular processes from the MS hits in (A).

Figure 4. Calcineurin-dependent phosphosites S86 and T172 of GAP-43 regulate α-synuclein-dependent pathobiology. **(A)** Representative western blot from primary embryonic rat cortical neurons transduced with either GFP, or GFP fusions of GAP-43 Wild type (WT), phosphoablative (S86A,T172A) or phosphomimetic (S86E,T172E) mutants of the CaN-dependent phosphorylation sites, or the previously established PKC-dependent site (S41) in phosphoablative, S41A, or phosphomimetic, S41D, mutant form, alone or in combination with αSyn A53T. Actin serves as a loading control. N=3. **(B-C)** Representative images from (A) immunostained for the neuronal marker MAP2 and quantified for MAP2. **(D)** Quantification of ATP levels from cultures in (A). Experiments in (A-D) N=3. **(E)** Representative western blot for PSD-95, GAP-43 GFP from cultures in (A) and quantitation of PSD95 signal/actin, the loading control **(F)**. ANOVA with post-hoc Tukey test.; *<0.05; **<0.01; ***<0.001.

REFERENCES

1 Alafuzoff, I. & Hartikainen, P. Alpha-synucleinopathies. Handb Clin Neurol 145, 339-353, (2017),

2 Chan, C. S. et al. 'Rejuvenation' protects neurons in mouse models of Parkinson's disease. Nature 447, 1081-1086, (2007),

3 Dufty, B. M. et al. Calpain-cleavage of alpha-synuclein: connecting proteolytic processing to disease-linked aggregation. Am J Pathol 170, 1725-1738, (2007), PMC1854966.

4 Surmeier, D. J., Obeso, J. A. & Halliday, G. M. Selective neuronal vulnerability in Parkinson disease. Nat Rev Neurosci 18, 101-113, (2017), PMC5564322.

5 Yuan, H. H., Chen, R. J., Zhu, Y. H., Peng, C. L. & Zhu, X. R. The neuroprotective effect of overexpression of calbindin-D(28k) in an animal model of Parkinson's disease. Mol Neurobiol 47, 117-122, (2013),

6 Caraveo, G. et al. FKBP12 contributes to alpha-synuclein toxicity by regulating the calcineurin-dependent phosphoproteome. Proc Natl Acad Sci U S A 114, E11313-E11322, (2017), PMC5748183.

7 Guzman, J. N. et al. Oxidant stress evoked by pacemaking in dopaminergic neurons is attenuated by DJ-1. Nature 468, 696-700, (2010), 4465557.

8 Hurley, M. J., Brandon, B., Gentleman, S. M. & Dexter, D. T. Parkinson's disease is associated with altered expression of CaV1 channels and calcium-binding proteins. Brain 136, 2077-2097, (2013), PMC3461271.

9 Surmeier, D. J., Guzman, J. N., Sanchez-Padilla, J. & Goldberg, J. A. The origins of oxidant stress in Parkinson's disease and therapeutic strategies. Antioxid Redox Signal 14, 1289-1301, (2010), 3048813.

10 Goldberg, J. A. et al. Calcium entry induces mitochondrial oxidant stress in vagal neurons at risk in Parkinson's disease. Nat Neurosci 15, 1414-1421, (2012), PMC3461271.

11 Surmeier, D. J. et al. Calcium and Parkinson's disease. Biochem Biophys Res Commun, (2016),

12 Caraveo, G. et al. Calcineurin determines toxic versus beneficial responses to alpha-synuclein. Proc Natl Acad Sci U S A 111, E3544-3552, (2014), PMC4151770.

13 Martin, Z. S. et al. alpha-Synuclein oligomers oppose long-term potentiation and impair memory through a calcineurin-dependent mechanism: relevance to human synucleopathic diseases. J Neurochem 120, 440-452, (2012), PMC3253169.

14 Burbulla, L. F. et al. Dopamine oxidation mediates mitochondrial and lysosomal dysfunction in Parkinson's disease. Science 357, 1255-1261, (2017),

15 Tron, C. et al. Pharmacogenetics of Membrane Transporters of Tacrolimus in Solid Organ Transplantation. Clin Pharmacokinet, (2018),

16 Frey, D., Laux, T., Xu, L., Schneider, C. & Caroni, P. Shared and unique roles of CAP23 and GAP43 in actin regulation, neurite outgrowth, and anatomical plasticity. J Cell Biol 149, 1443-1454, (2000), PMC2175140.

17 Holahan, M. R. A Shift from a Pivotal to Supporting Role for the Growth-Associated Protein (GAP-43) in the Coordination of Axonal Structural and Functional Plasticity. Front Cell Neurosci 11, 266, (2017), PMC5583208.

18 Denny, J. B. Molecular mechanisms, biological actions, and neuropharmacology of the growth-associated protein GAP-43. Curr Neuropharmacol 4, 293-304, (2006), PMC2475799.

19 Korshunova, I. et al. Characterization of BASP1-mediated neurite outgrowth. J Neurosci Res 86, 2201-2213, (2008),

20 Chan, S. Y., Murakami, K. & Routtenberg, A. Phosphoprotein F1: purification and characterization of a brain kinase C substrate related to plasticity. J Neurosci 6, 3618-3627, (1986), PMC6568663.
21 Skene, J. H. Axonal growth-associated proteins. Annu Rev Neurosci 12, 127-156, (1989),
22 Liu, Y. C. & Storm, D. R. Dephosphorylation of neuromodulin by calcineurin. J Biol Chem 264, 12800-12804, (1989),
23 Nielander, H. B. et al. Mutation of serine 41 in the neuron-specific protein B-50 (GAP-43) prohibits phosphorylation by protein kinase C. J Neurochem 55, 1442-1445, (1990),
24 Greene, L. A. & Tischler, A. S. Establishment of a noradrenergic clonal line of rat adrenal pheochromocytoma cells which respond to nerve growth factor. Proc Natl Acad Sci U S A 73, 2424-2428, (1976), PMC430592.
25 Polymeropoulos, M. H. et al. Mutation in the alpha-synuclein gene identified in families with Parkinson's disease. Science 276, 2045-2047, (1997),
26 Caraveo, G. et al. FKBP12 contributes to alpha-synuclein toxicity by regulating the calcineurin-dependent phosphoproteome. Proc Natl Acad Sci U S A, (2017),
27 Lundby, A. et al. Quantitative maps of protein phosphorylation sites across 14 different rat organs and tissues. Nat Commun 3, 876, (2012), PMC3621391.
28 Biarc, J., Chalkley, R. J., Burlingame, A. L. & Bradshaw, R. A. The induction of serine/threonine protein phosphorylations by a PDGFR/TrkA chimera in stably transfected PC12 cells. Mol Cell Proteomics 11, 15-30, (2012), PMC3418849.
29 Spencer, S. A., Schuh, S. M., Liu, W. S. & Willard, M. B. GAP-43, a protein associated with axon growth, is phosphorylated at three sites in cultured neurons and rat brain. J Biol Chem 267, 9059-9064, (1992),
30 Slomnicki, L. P. et al. Requirement of Neuronal Ribosome Synthesis for Growth and Maintenance of the Dendritic Tree. J Biol Chem 291, 5721-5739, (2016), PMC4786710.
31 Jaworski, J., Spangler, S., Seeburg, D. P., Hoogenraad, C. C. & Sheng, M. Control of dendritic arborization by the phosphoinositide-3'-kinase-Akt-mammalian target of rapamycin pathway. J Neurosci 25, 11300-11312, (2005), PMC6725892.
32 Kwon, M., Fernandez, J. R., Zegarek, G. F., Lo, S. B. & Firestein, B. L. BDNF-promoted increases in proximal dendrites occur via CREB-dependent transcriptional regulation of cypin. J Neurosci 31, 9735-9745, (2011), PMC3139247.
33 Lesiak, A. et al. A genome-wide screen of CREB occupancy identifies the RhoA inhibitors Par6C and Rnd3 as regulators of BDNF-induced synaptogenesis. PLoS One 8, e64658, (2013), PMC3675129.
34 Kumar, V., Zhang, M. X., Swank, M. W., Kunz, J. & Wu, G. Y. Regulation of dendritic morphogenesis by Ras-PI3K-Akt-mTOR and Ras-MAPK signaling pathways. J Neurosci 25, 11288-11299, (2005), PMC6725910.
35 De Rubeis, S. et al. CYFIP1 coordinates mRNA translation and cytoskeleton remodeling to ensure proper dendritic spine formation. Neuron 79, 1169-1182, (2013), PMC3781321.
36 Gupta, S. K. et al. GAP-43 is essential for the neurotrophic effects of BDNF and positive AMPA receptor modulator S18986. Cell Death Differ 16, 624-637, (2009),
37 Palasz, E. et al. BDNF as a Promising Therapeutic Agent in Parkinson's Disease. Int J Mol Sci 21, (2020), PMC7037114.
38 Li, C. et al. Pilose Antler Extracts (PAEs) Protect against Neurodegeneration in 6-OHDA-Induced Parkinson's Disease Rat Models. Evid Based Complement Alternat Med 2019, 7276407, (2019), PMC6341246.
39 Tonges, L. et al. Alpha-synuclein mutations impair axonal regeneration in models of Parkinson's disease. Front Aging Neurosci 6, 239, (2014), PMC4159996.
40 Sjogren, M. et al. CSF levels of tau, beta-amyloid(1-42) and GAP-43 in frontotemporal dementia, other types of dementia and normal aging. J Neural Transm (Vienna) 107, 563-579, (2000),

41 Saal, K. A. et al. Altered Expression of Growth Associated Protein-43 and Rho Kinase in Human Patients with Parkinson's Disease. Brain Pathol 27, 13-25, (2017),
42 Lesuisse, C. & Martin, L. J. Long-term culture of mouse cortical neurons as a model for neuronal development, aging, and death. J Neurobiol 51, 9-23, (2002),
43 Pacifici, M. & Peruzzi, F. Isolation and culture of rat embryonic neural cells: a quick protocol. J Vis Exp, e3965, (2012), PMC3466945.
44 Park, I. H., Lerou, P. H., Zhao, R., Huo, H. & Daley, G. Q. Generation of human-induced pluripotent stem cells. Nat Protoc 3, 1180-1186, (2008),
45 Schindelin, J. et al. Fiji: an open-source platform for biological-image analysis. Nat Methods 9, 676-682, (2012), PMC3855844.

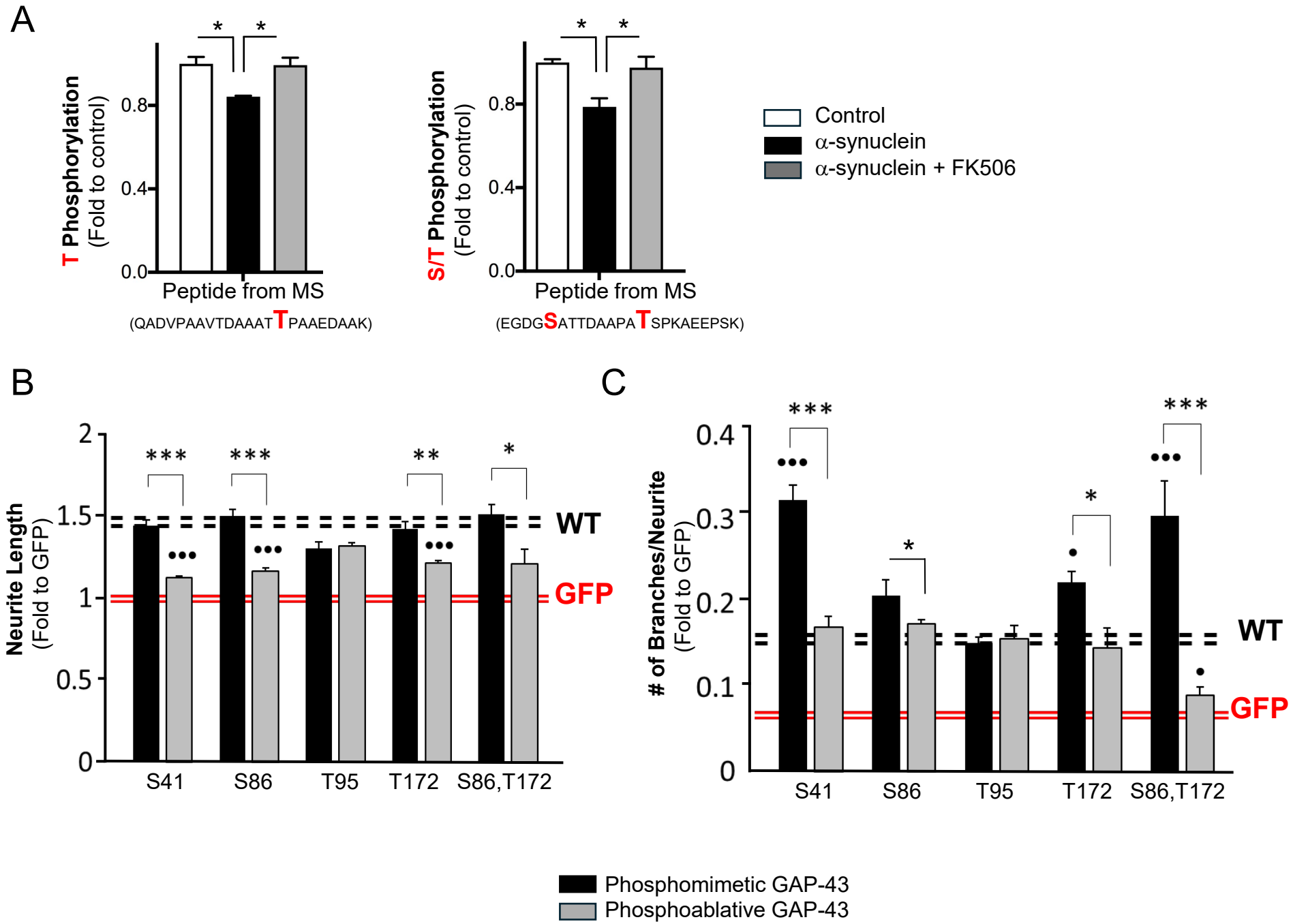
A
T Phosphorylation
(Fold to control)
0.0
0.4
0.8
*
*
Peptide from MS
(QADVPAAVTDAAATTPAAEDAAK)
S/T Phosphorylation
(Fold to control)
0.0
0.4
0.8
*
*
Peptide from MS
(EGDGSATTDAAPATSPKAEEPSK)
Control
α-synuclein
α-synuclein + FK506
B
Neurite Length
(Fold to GFP)
0
0.5
1
1.5
2
***
***
**
*
•••
•••
•••
WT
GFP
S41
S86
T95
T172
S86,T172
C
# of Branches/Neurite
(Fold to GFP)
0
0.1
0.2
0.3
0.4
***
***
*
*
•••
•••
•
•
WT
GFP
S41
S86
T95
T172
S86,T172
Phosphomimetic GAP-43
Phosphoablative GAP-43

Figure 1

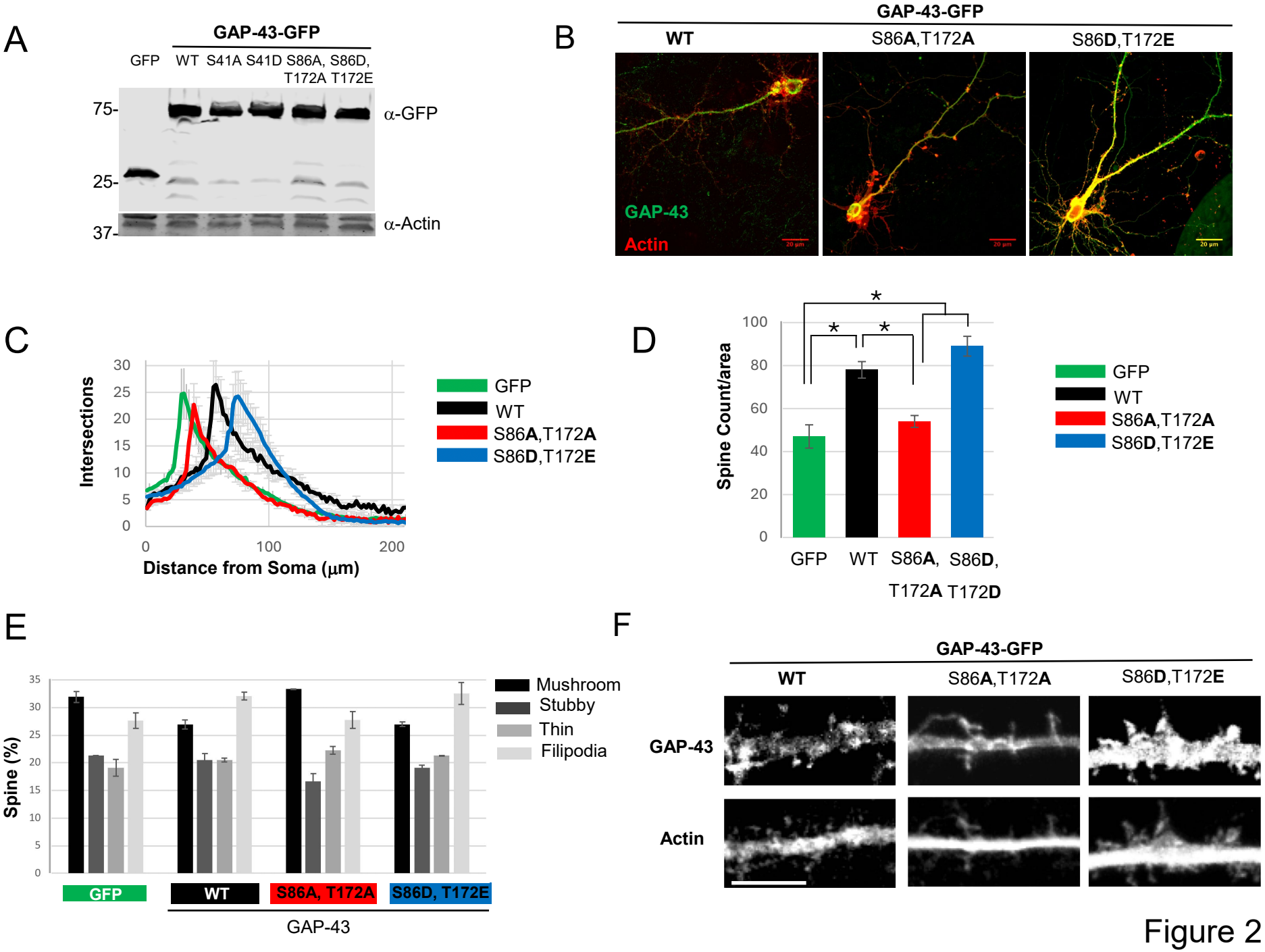
A
GAP-43-GFP
GFP
WT
S41A
S41D
S86A, T172A
S86D, T172E
75-
25-
37-
α-GFP
α-Actin
B
GAP-43-GFP
WT
S86A,T172A
S86D,T172E
GAP-43
Actin
C
Intersections
Distance from Soma (μm)
GFP
WT
S86A,T172A
S86D,T172E
D
Spine Count/area
GFP
WT
S86A, T172A
S86D, T172D
E
Spine (%)
Mushroom
Stubby
Thin
Filipodia
GFP
WT
S86A, T172A
S86D, T172E
GAP-43
F
GAP-43-GFP
WT
S86A,T172A
S86D,T172E
GAP-43
Actin

Figure 2

A

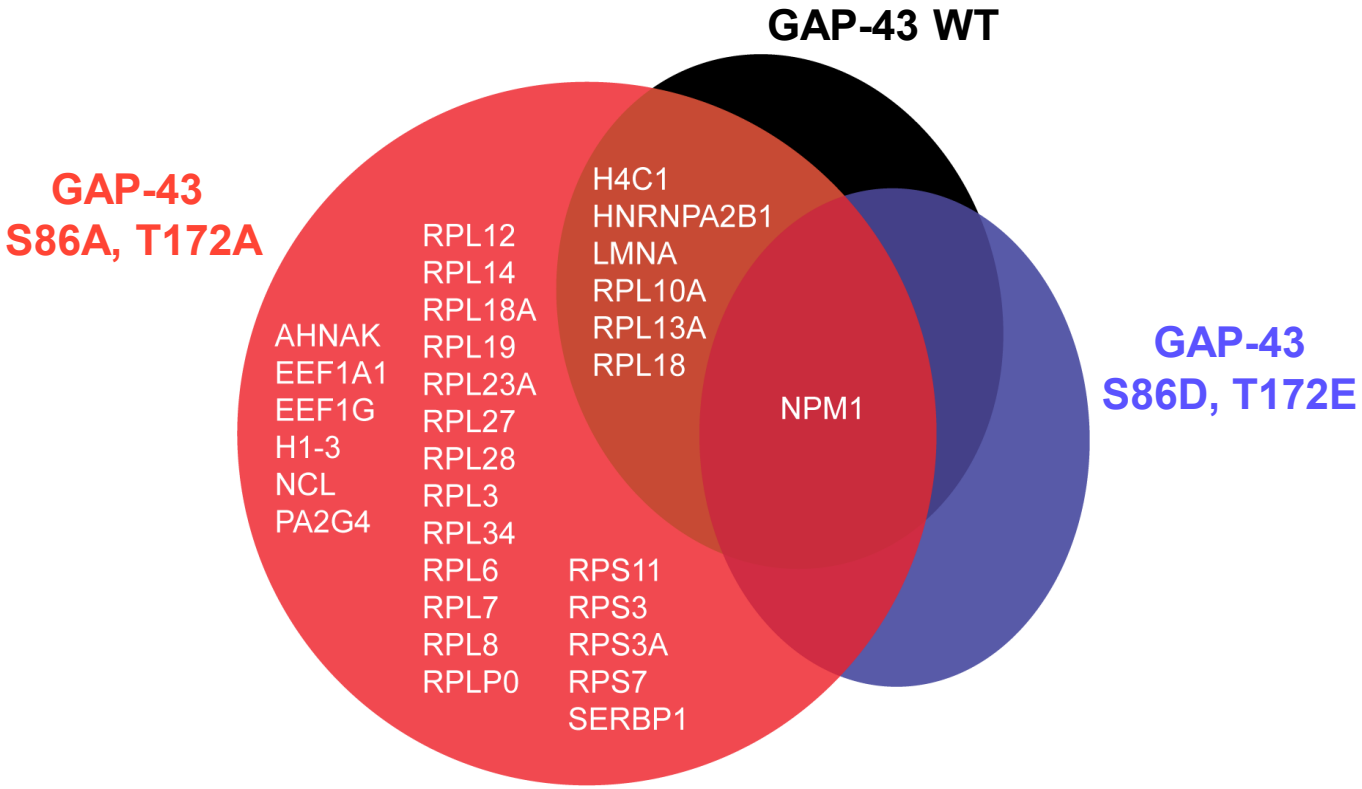
GAP-43 WT
GAP-43
S86A, T172A
GAP-43
S86D, T172E
AHNAK
EEF1A1
EEF1G
H1-3
NCL
PA2G4
RPL12
RPL14
RPL18A
RPL19
RPL23A
RPL27
RPL28
RPL3
RPL34
RPL6
RPL7
RPL8
RPLP0
RPS11
RPS3
RPS3A
RPS7
SERBP1
H4C1
HNRNPA2B1
LMNA
RPL10A
RPL13A
RPL18
NPM1

B

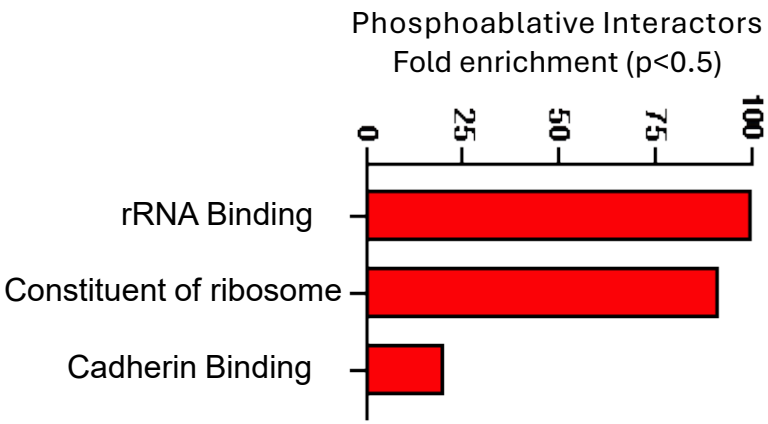
Phosphoablative Interactors
Fold enrichment (p<0.5)
0
25
50
75
100
rRNA Binding
Constituent of ribosome
Cadherin Binding

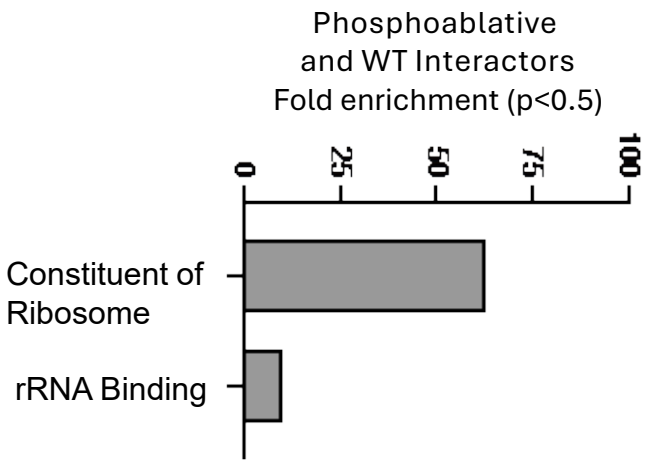
Phosphoablative
and WT Interactors
Fold enrichment (p<0.5)
0
25
50
75
100
Constituent of
Ribosome
rRNA Binding

Figure 3

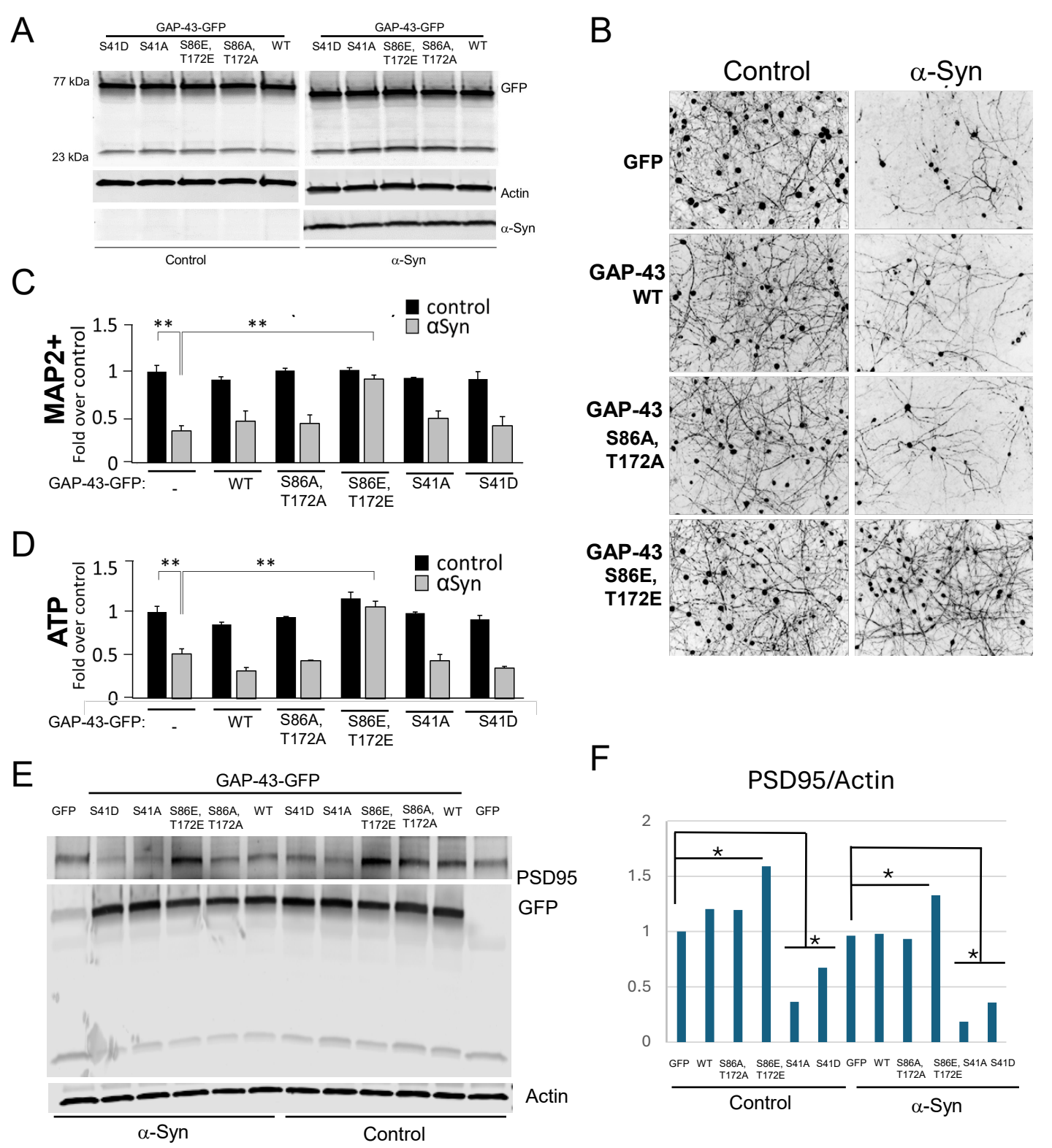
A
GAP-43-GFP
S41D S41A S86E, T172E S86A, T172A WT
GAP-43-GFP
S41D S41A S86E, T172E S86A, T172A WT
77 kDa
23 kDa
GFP
Actin
α-Syn
Control
α-Syn
B
Control
α-Syn
GFP
GAP-43 WT
GAP-43 S86A, T172A
GAP-43 S86E, T172E
C
MAP2+
Fold over control
control
αSyn
1.5
1
0.5
0
**
**
GAP-43-GFP:
-
WT
S86A, T172A
S86E, T172E
S41A
S41D
D
ATP
Fold over control
control
αSyn
1.5
1
0.5
0
**
**
GAP-43-GFP:
-
WT
S86A, T172A
S86E, T172E
S41A
S41D
E
GAP-43-GFP
GFP S41D S41A S86E, T172E S86A, T172A WT S41D S41A S86E, T172E S86A, T172A WT GFP
PSD95
GFP
Actin
α-Syn
Control
F
PSD95/Actin
2
1.5
1
0.5
0
*
*
*
*
GFP WT S86A, T172A S86E, T172E S41A S41D GFP WT S86A, T172A S86E, T172E S41A S41D
Control
α-Syn

Figure 4